Supplemental Text

GPS data processing

All of the GPS data used in this study are freely available on the internet. We downloaded daily RINEX files from the UNAVCO, Inc. archive (data-out.unavco.org). The data were processed with the GIPSY-OASIS II software package from the Jet Propulsion Laboratory (JPL) as a part of a global solution that includes over 3500 stations worldwide. Station coordinates were estimated every 24 hours using the Precise Point Positioning (PPP) method (*Zumberge et al*., 1997). Ionosphere-free combinations of carrier phase and pseudorange were processed every 5 minutes. Estimated parameters included a tropospheric zenith bias and two gradient parameters estimated as random-walk processes, and station clocks estimated as a white-noise process. We resolved ambiguities in carrier phase across the entire global network by automatic selection of the ionospheric- or pseudorange-widelane method using the rapid Ambizap algorithm which is based on a fixed-point theorem that approximates a full-network resolution to better than 1 mm (*Blewitt*, 2008). Satellite orbit and clock parameters were provided by JPL, who determine these parameters in a global fiducial-free analysis using a subset of the available IGS core stations as tracking sites. To ensure that the *a priori* position estimates did not have an impact on positions, we used an iterative procedure where we first solved for the daily coordinates for each site and then used these coordinates for the *a priori* coordinates in the final solution. We deleted data that were immediately recognizable outliers in the time series, i.e. those positions more than 10 meters from the median position for each site, or positions with uncertainties in any (x, y, or z) coordinate greater than 10 mm. Sites that exhibited significant gaps, a larger number of steps in their time series, or time series less than 7 years long were not included in the analysis.

Reference Frame Alignment

The daily GPS solutions were aligned with a reference frame co-rotating with the rigid interior of North America (NA), where reference frame sites were selected to avoid areas subject to significant post-glacial isostatic adjustment (GIA). In the first step daily solutions were aligned to ITRF2005 by applying a seven parameter transformation (3 rotations, 3 translations and a scale component) obtained online from JPL (sideshow.jpl.nasa.gov). In a subsequent 3 parameter rotation the daily solutions were aligned to minimize the horizontal velocity at 16 stations on the interior of the NA plate, all of which are located away from the peripheral bulge associated with isostatic adjustment. The 16 GPS sites are BRMU, BRTW, DQUA, FBYN, GODE, HAMM, HLFX, JTNT, MACC, MBWW, NPRI, PLTC, PRCO, STJO, WLCI, WNCI. In a third step, 21 long running and stable sites in the Great Basin, mostly from the BARGEN network, were used to define a 7-parameter spatial filter that removes common-mode noise (*Wdowinski et al*., 1997). This type of noise is common to all sites in the network and includes daily residual translations of the regional network that might arise from orbit error, or other sources of bias common to the network. The sites chosen to define this filter are ALAM, ARGU, BEAT, CAST, DYER, ECHO, ELKO, FERN, FOOT, FRED, GARL, GOSH, LIND, NEWS, RAIL, RUBY, SHIN, SMEL, TONO, TUNG, UPSA

(Figure S5). Because this filtering is applied on the scale of the entire Great Basin, based on sites north of the effects of the relaxation from the Hector Mine and Landers earthquakes, it is not strongly distorted by the transient motions.

Captions for Auxiliary Figures.

Figure S1. Back dots are change in GPS velocity in NA reference frame between first (2000.0 to 2002.5) and last (2006.0 to 2008.5). Uncertainties are 2σ based on estimate of 0.2 mm/yr rate uncertainty (see text). Red dots show same change in rates after correction for viscoelastic relaxation has been applied to GPS time series.

Figure S2. Viscoelastic stratification used in model. A) Elastic upper crust extends from surface to 15 km depth, lower crust and upper mantle are Maxwell viscoelastic with indicated possible ranges for viscosity explored in this study. B) Depth dependence of elastic shear and bulk moduli.

Figure S3. Rates inferred from viscoelastic model with $\eta_{LC}= 10^{19.5}$ Pa s, $\eta_{UM}=10^{18.5}$ Pa s on a regular grid for years 2002 – 2008 for A) all events, B) Hector Mine only, C) Landers only, D) Owens Valley, E) Kern County, F) Ft Tejon, G) Cedar Mountain, H) Little Skull. See Table S1 for earthquake properties. Majenta line segments are fault traces used in viscoelastic modeling. Green triangles are location where VISCO1D relaxation model was evaluated prior to interpolation for plotting rates in this figure. Box indicates location of YM GPS cluster. Note change in vector scale between figures.

Figure S4. Same as Figure 1B, except 2.5 year long interval rates are shown in gray, and velocities obtained from time series corrected for all the events in Table 1 are shown at each site (black vectors). Topography and faults have been omitted for clarity.

Figure S5. Region containing study area (black box is area of Figure 1A) showing locations of GPS sites used to define the Great Basin-spatial-scale regional filtering.

Auxiliary References

Beanland, S., and M. M. Clark (1994), The Owens Valley fault zone, eastern California, and surface rupture associated with the 1872 earthquake, *U.S. Geological Survey Bulletin*, *1982*, 1-29.

Bell, J. W., C. M. dePolo, A. R. Ramelli, A. M. Sarna-Wojcicki, and C. E. Meyer (1999), Surface faulting and paleoseismic history of the 1932 Cedar Mountain earthquake area, west-central Nevada, and implications for modern tectonics of the Walker Lane, *GSA Bulletin*, *111*, 6, 791-807.

Blewitt, G. (2008), Fixed-Point theorems of GPS carrier phase ambiguity resolution and their application to massive network processing: "Ambizap", *J. Geophys. Res.*, *113, B12410, doi:10.1029/2008JB005736*.

Doser, D. I. (1988), Source parameters of earthquakes in the Nevada seismic zone, 1915-1943, *J. Geophys. Res.*, *93*, B12, 15,001-015,015.

Fialko, Y., M. Simons, and D. Agnew (2001), The complete (3-D) surface displacement field in the epicentral area of the 1999 M(w)7.1 Hector Mine earthquake, California, from space geodetic observations, *Geophys. Res. Lett.*, *28*, 16, 3063-3066.

Fialko, Y. (2004), Probing the mechanical properties of seismically active crust with space geodesy: Study of the coseismic deformation due to the 1992 M(w)7.3 Landers (southern California) earthquake, *J. Geophys. Res., 109*, B03307, doi:10.1029/2003JB002756.

Lohman, R. B., M. Simons, and B. Savage (2002), Location and mechanism of the Little Skull Mountain earthquake as constrained by satellite radar interferometry and seismic waveform modeling, *J. Geophys. Res.*, *107*, B6, 2118, 10.1029/2001JB000627.

Sieh, K. E. (1978), Slip Along San-Andreas Fault Associated with Great 1857 Earthquake, *Bull. Seis. Soc. Am.*, *68*, 5, 1421-1448.

Smith, K. D., J. N. Brune, D. M. dePolo, M. K. Savage, R. Anooshehpoor, and A. F. Sheehan (2000), The 1992 Little Skull Mountain earthquake sequence, southern Nevada test site, in *Geologic and geophysical characterization studies of Yucca Mountain, Nevada, A potential high-level radioactive waste repository*, edited by J. W. Whitney and W. R. Keefer, U.S. Geological Survey, U.S. Department of the Interior.

Stein, R. S., and W. Thatcher (1981), Seismic and aseismic deformation associated with the 1952 Kern County, California, earthquake and relationship to the Quaternary history of the White Wolf Fault, *J. Geophys. Res.*, *86*, B6, 4913-4928.

Wdowinski, S., Y. Bock, J. Zhang, P. Fang, and J. Genrich (1997), Southern California permanent GPS geodetic array: Spatial filtering of daily positions for estimating coseismic and postseismic displacements induced by the 1992 Landers earthquake, *J. Geophys. Res.*, *102*, B8, 18,057-018,070.

Zumberge, J. F., M. B. Heflin, D. C. Jefferson, M. M. Watkins, and F. H. Webb (1997), Precise point positioning for the efficient and robust analysis of GPS data from large networks, *J. Geophys. Res.*, *102*, B3, 5005-5017.

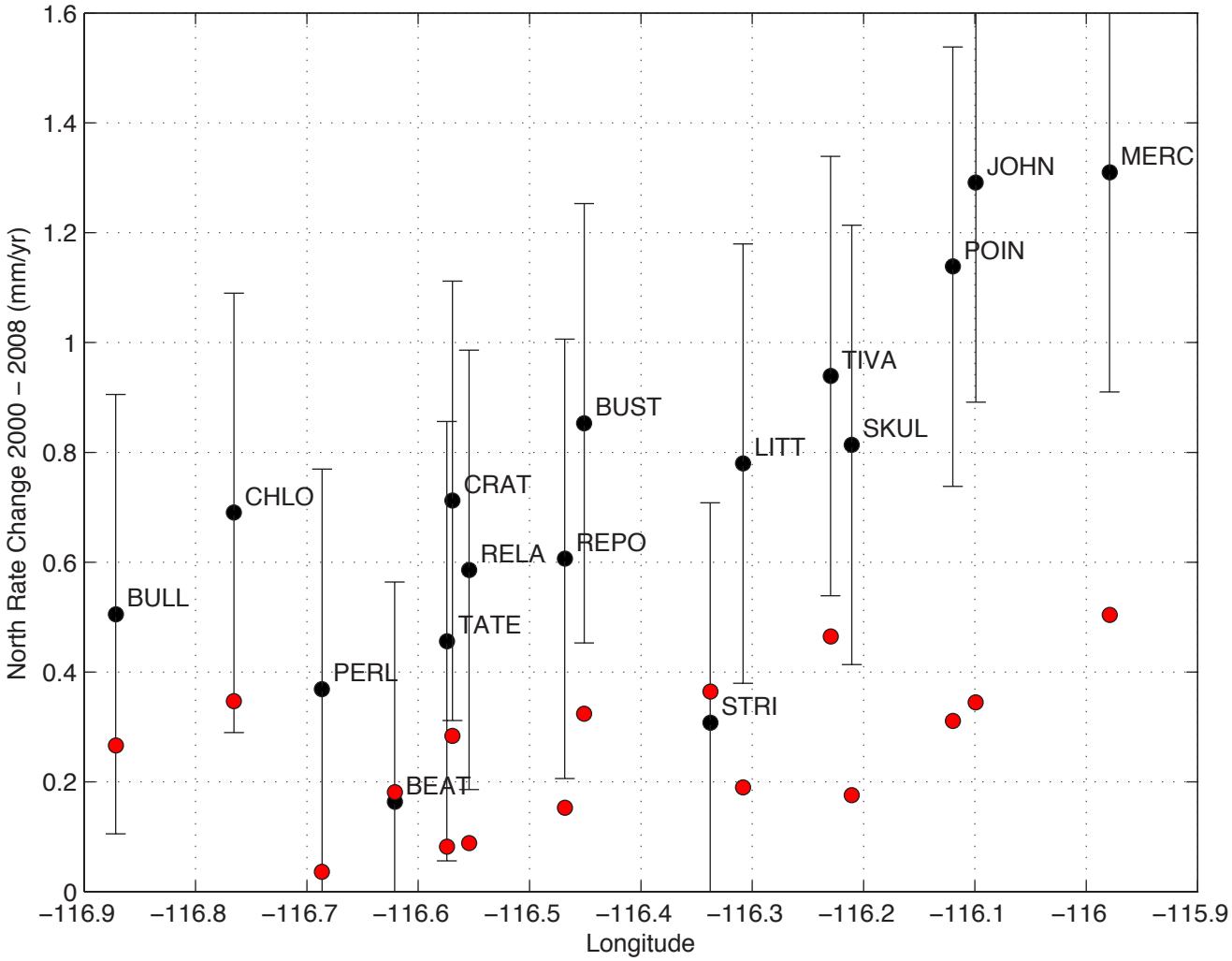

Figure S1: Hammond et al., 2010

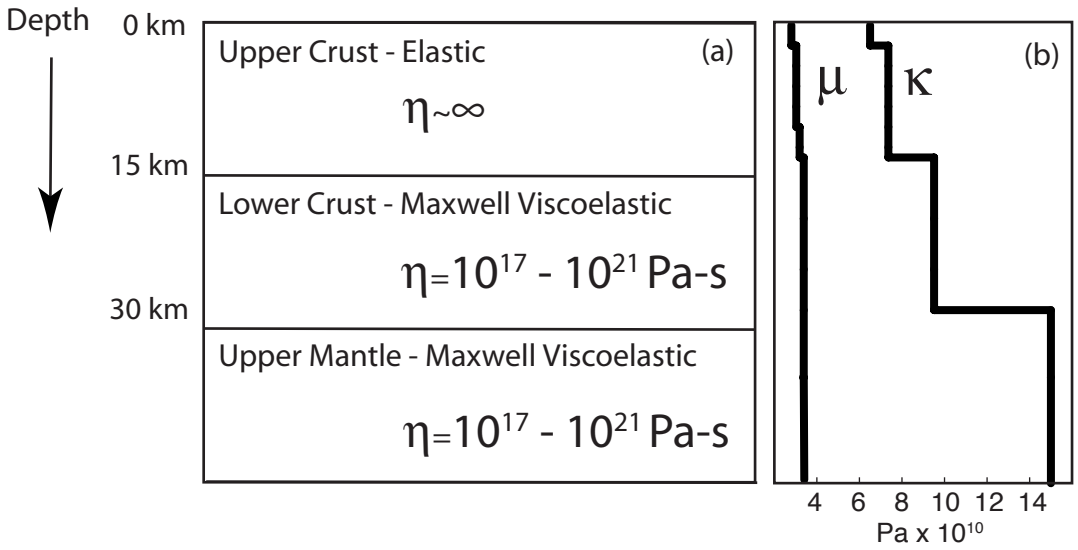

Figure S2, Hammond et al, 2010

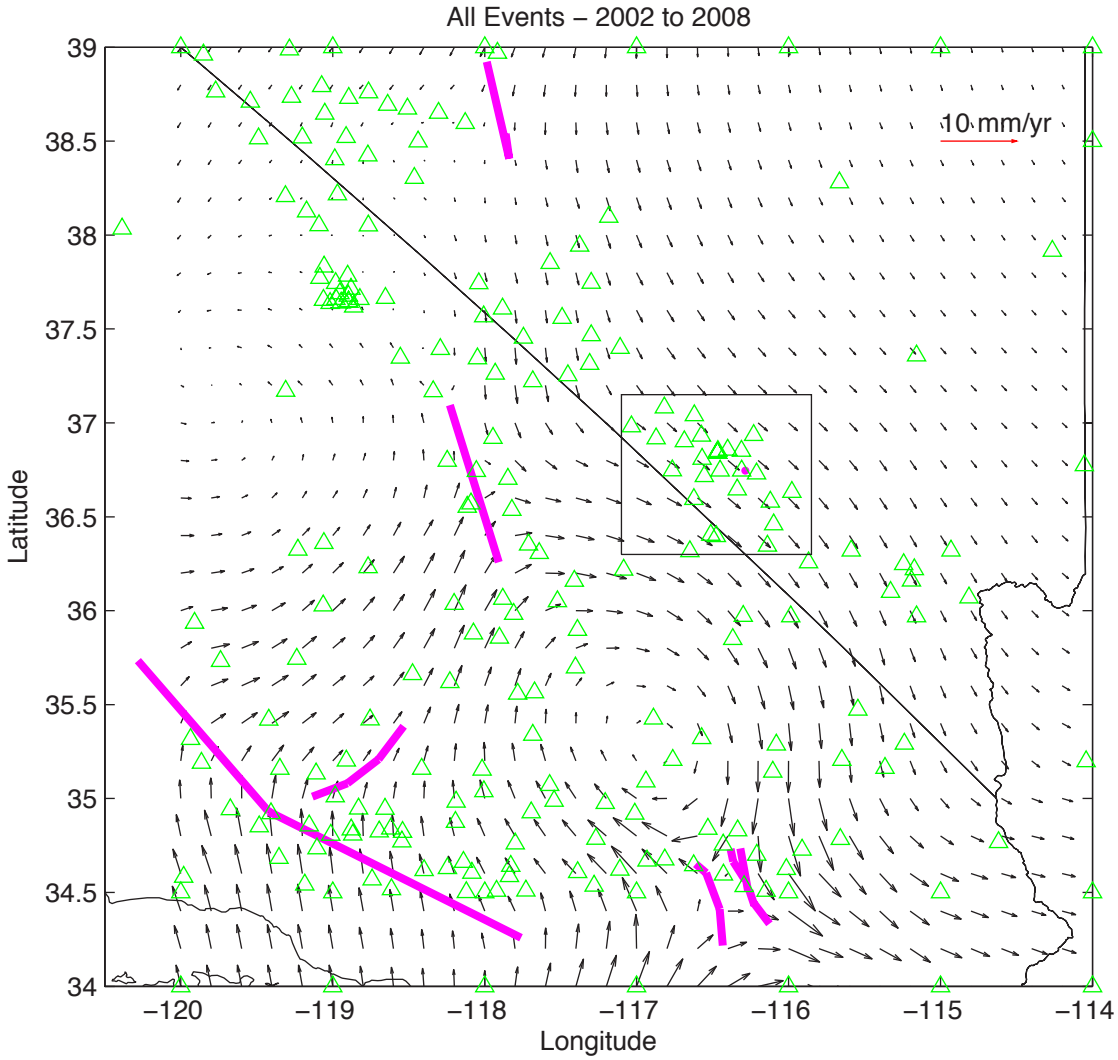

Figure S3A - Hammond et al., 2010

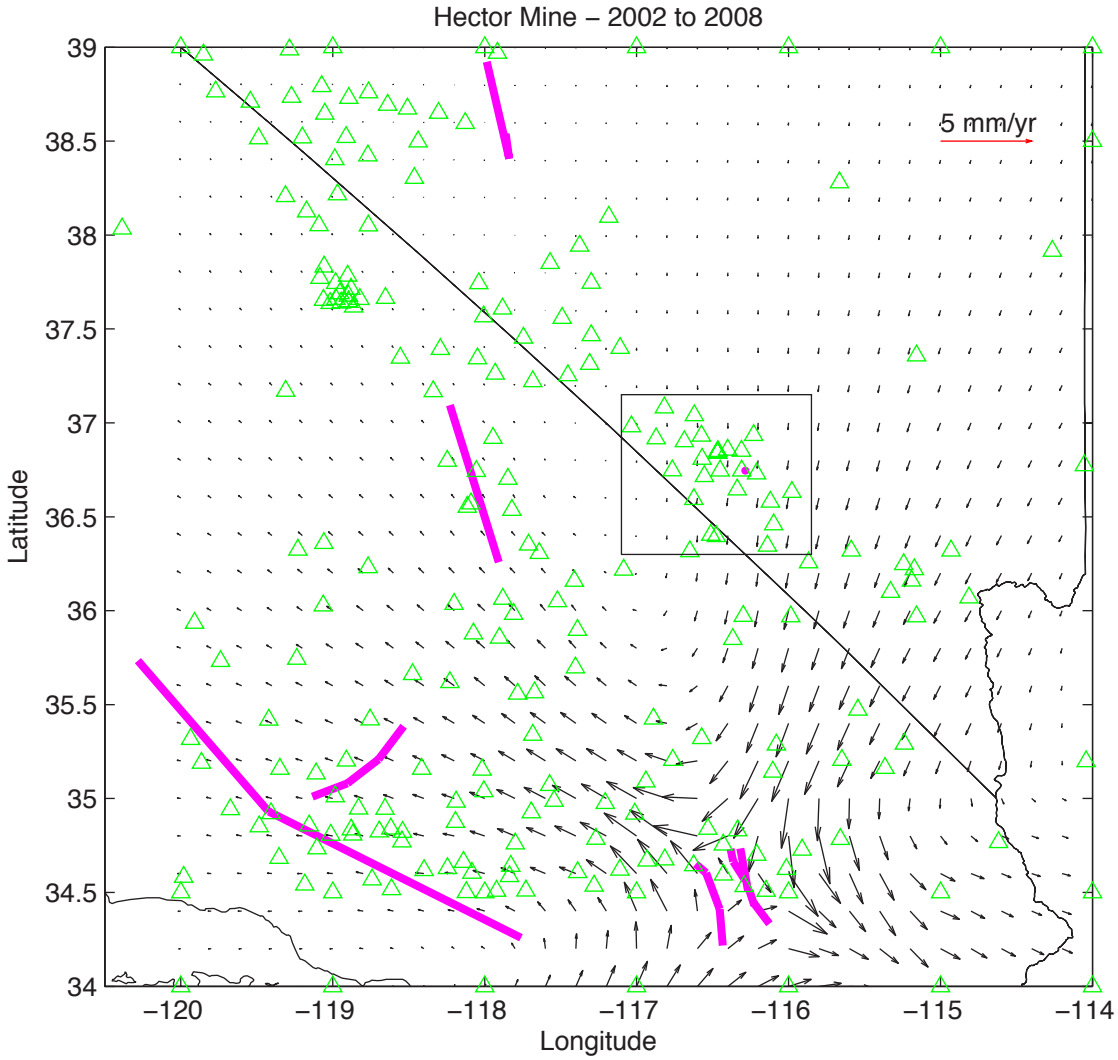

Figure S3B - Hammond et al., 2010

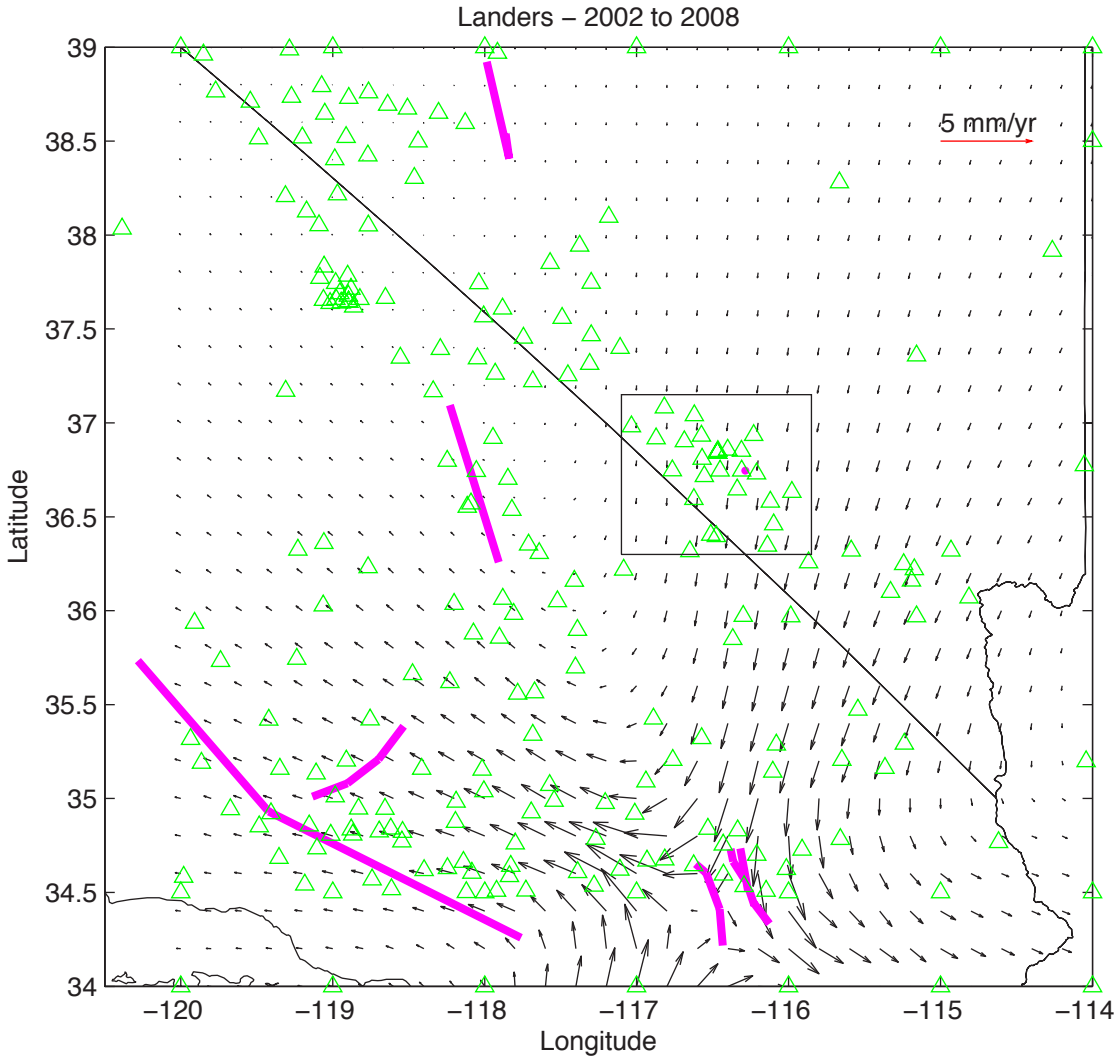

Figure S3C - Hammond et al., 2010

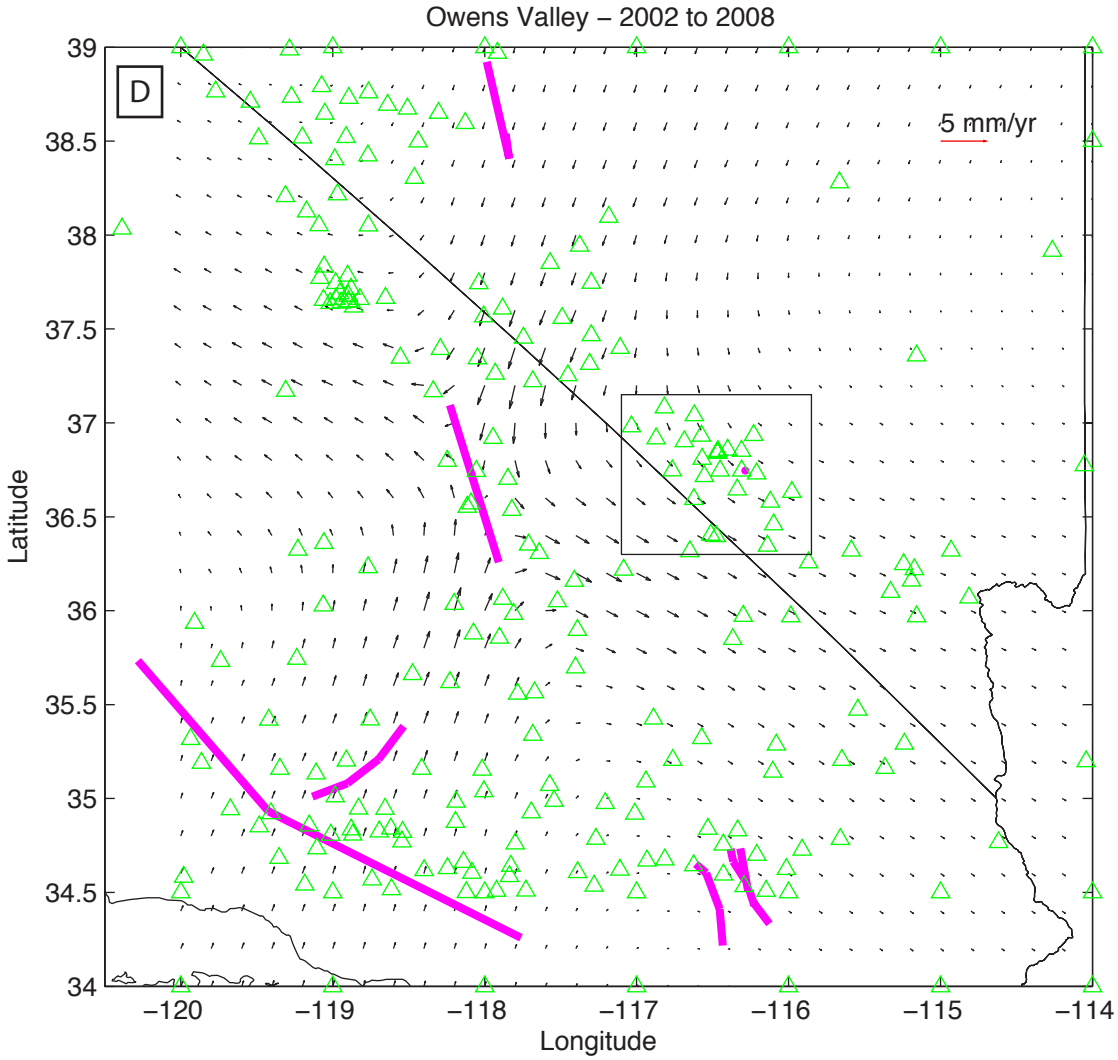

Figure S3D - Hammond et al., 2010

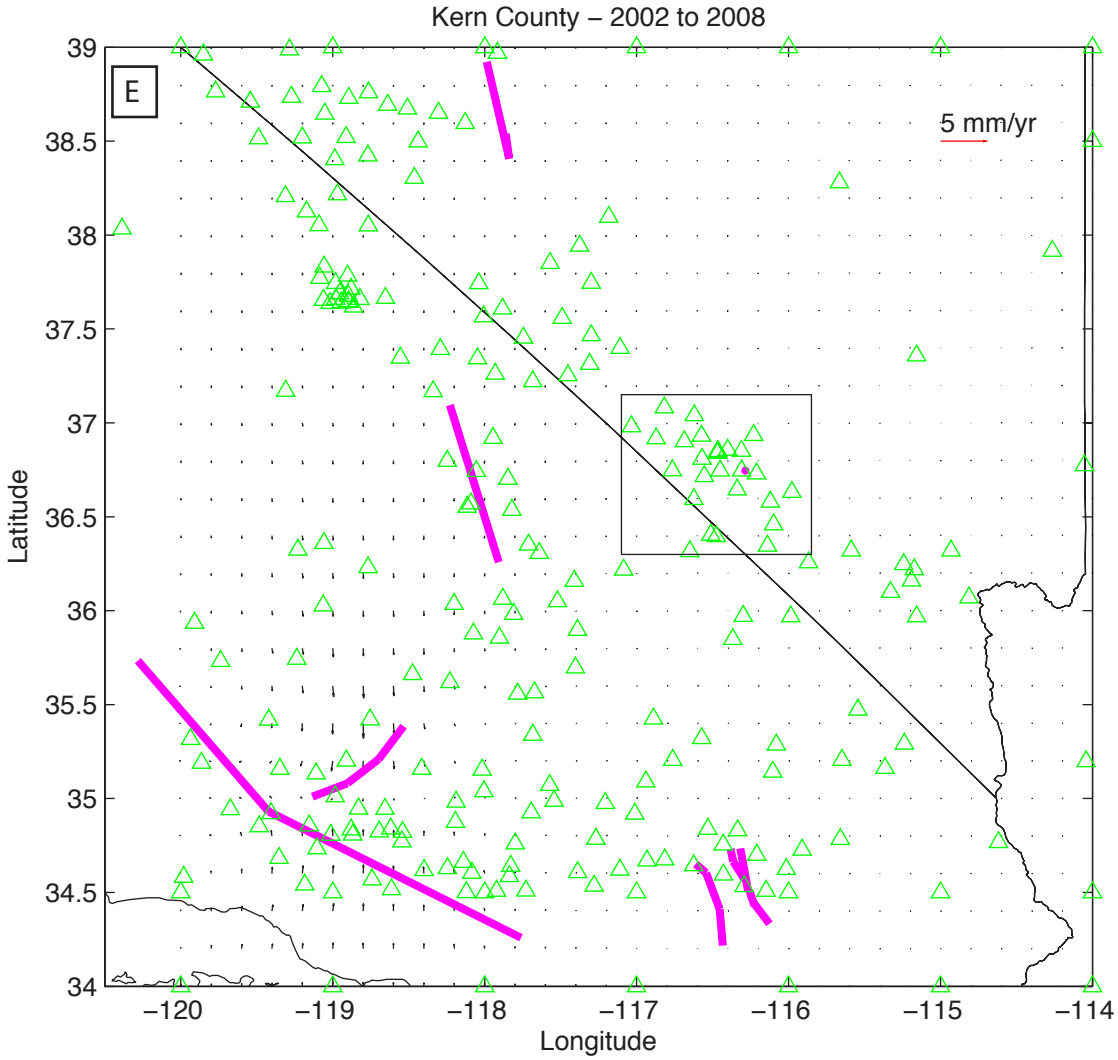

Figure S3E - Hammond et al., 2010

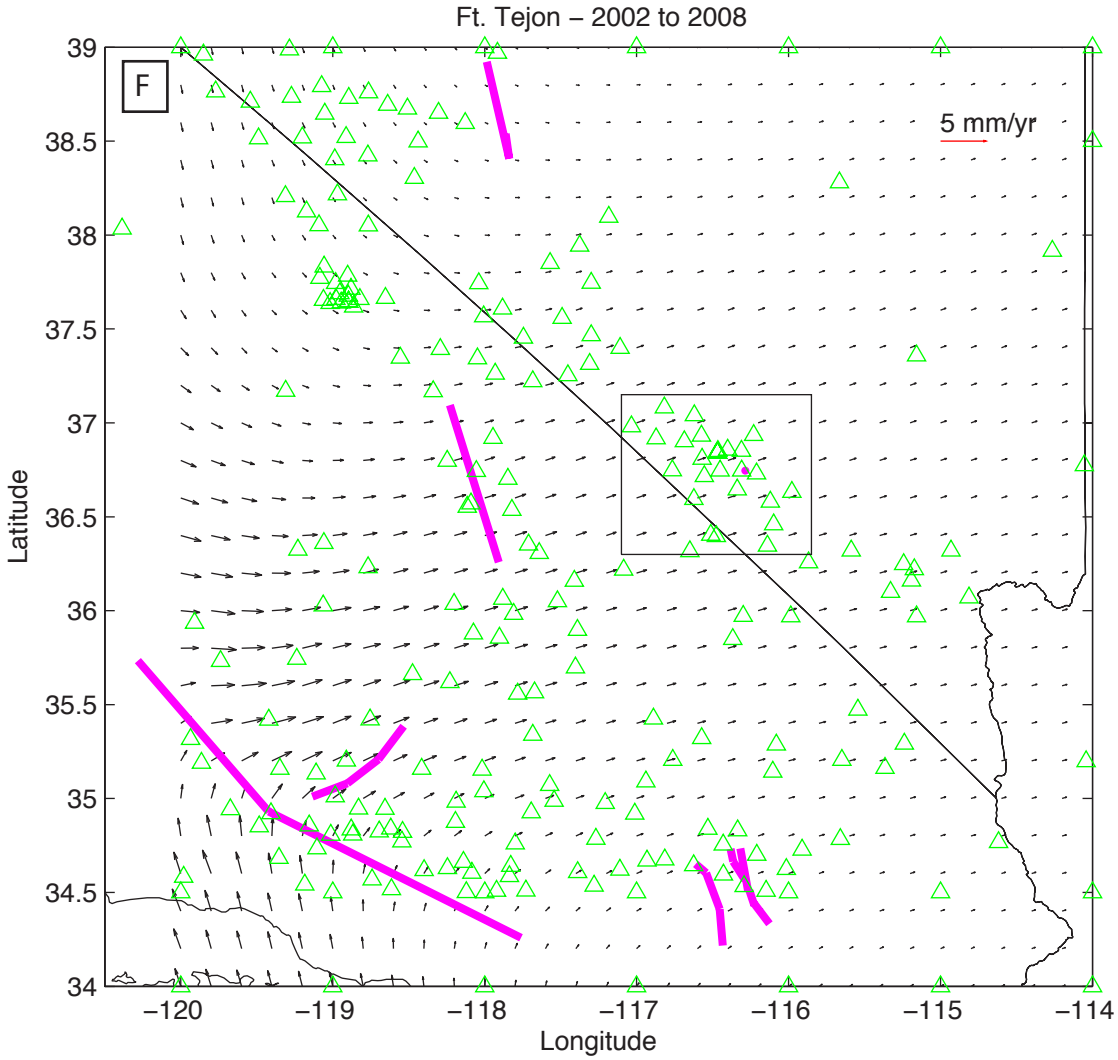

Figure S3F - Hammond et al., 2010

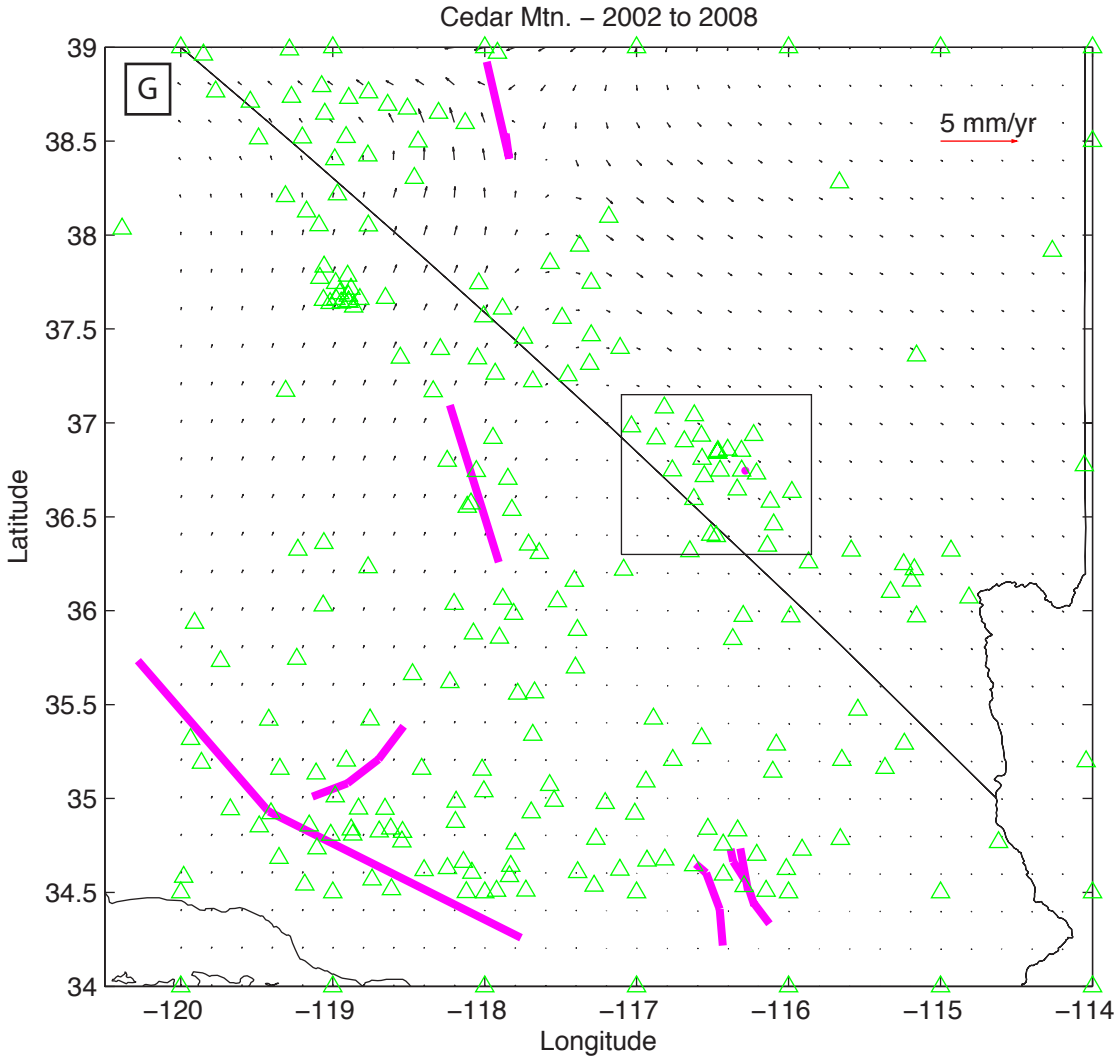

Figure S3G - Hammond et al., 2010

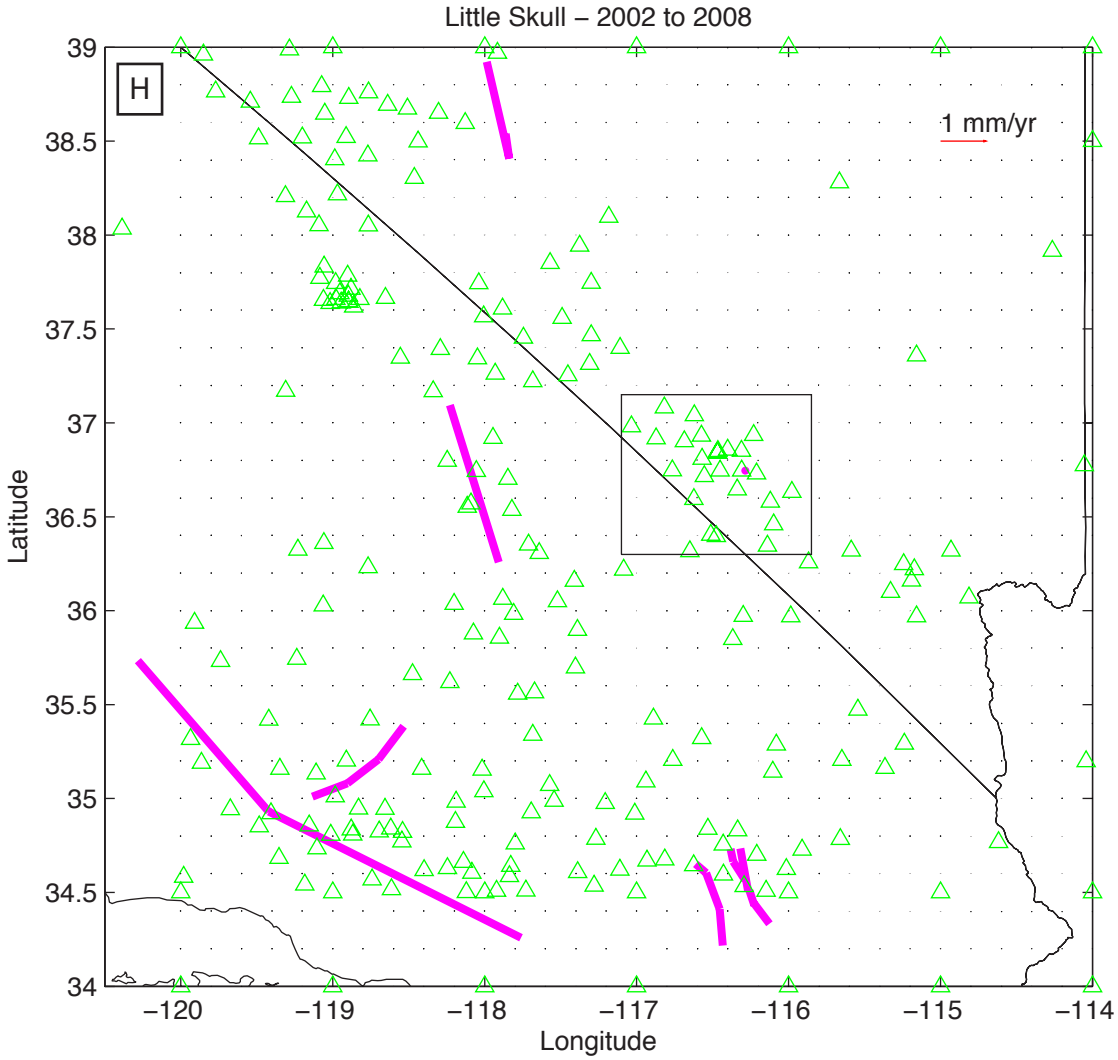

Figure S3H - Hammond et al., 2010

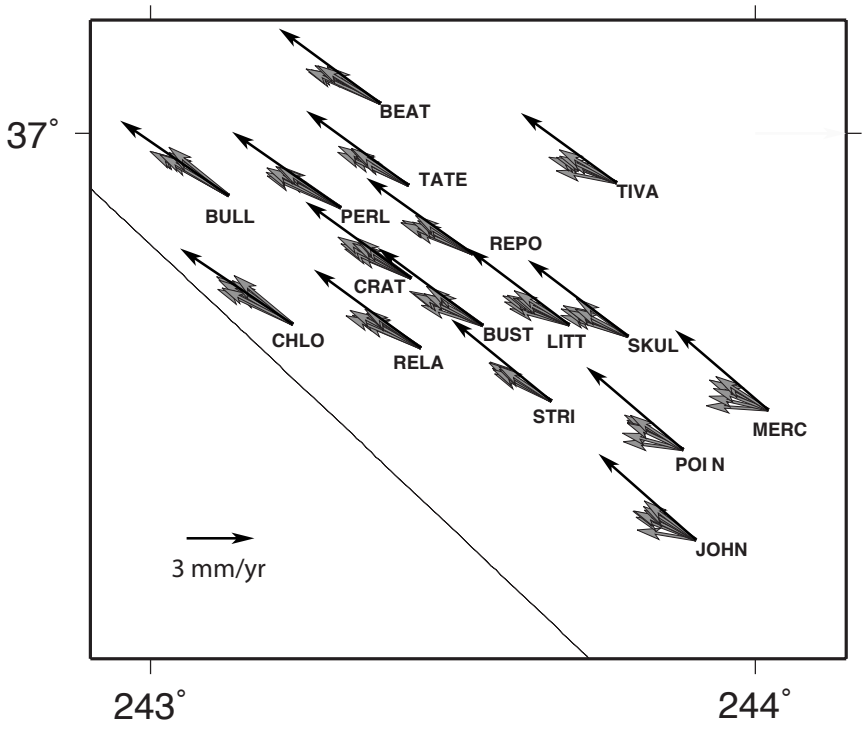

Figure S4, Hammond et al., 2010

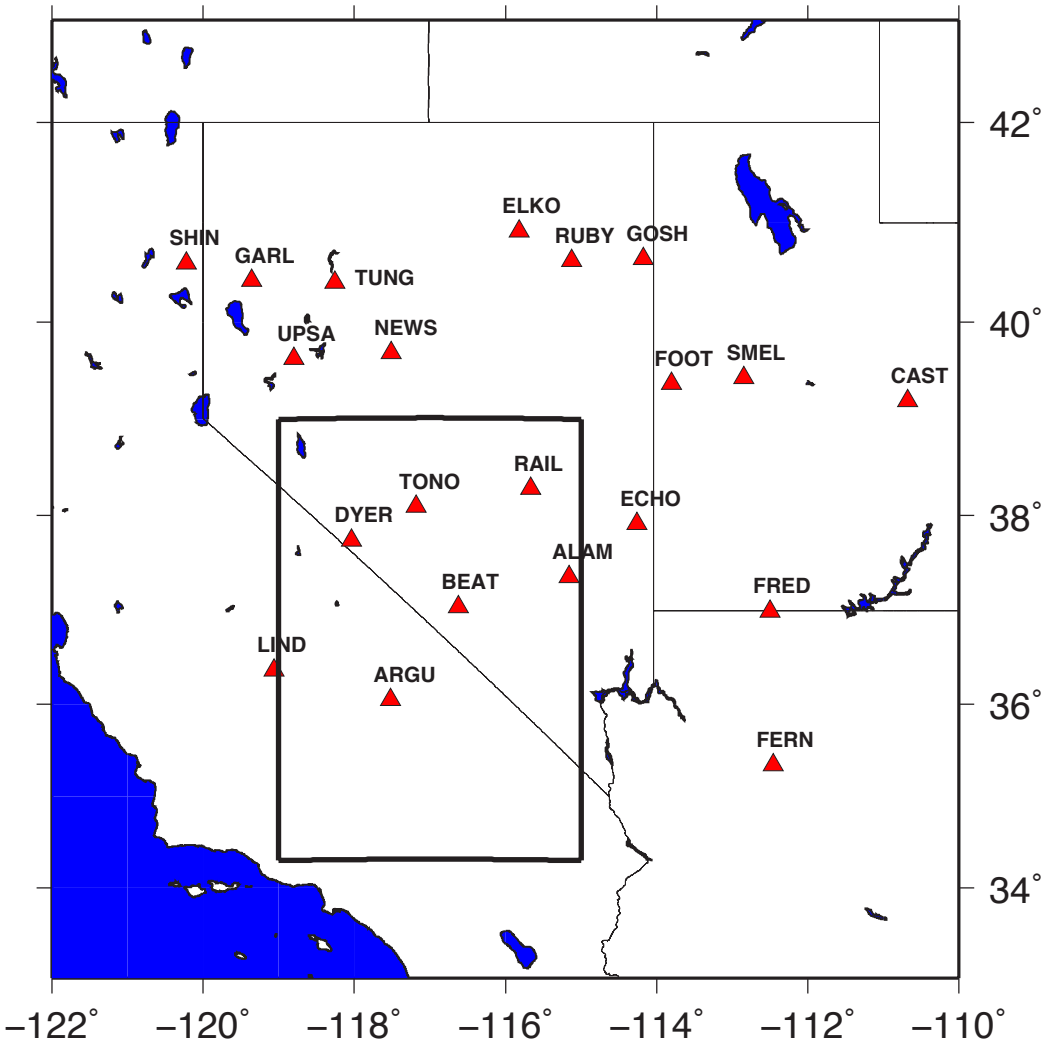

Figure S5 - Hammond et al.,2010

Table 1. Source Parameters of Earthquake Events

Event	Year	Top Depth (km)	Bottom Depth (km)	Dip (degrees)	Latitude (degrees)	Longitude (degrees)	Length (km)	Strike (degrees)	Rake (degrees)	Slip (meters)	Predominant Style
OwensValley[a]	1872.236	0	15	90	37.094	-118.229	100	339	180	6.0	Strike Slip
Landers[b]	1992.492	0	15	90	34.604	-116.54348	9.3	305	180	3.0	Strike Slip
	1992.492	0	15	90	34.411	-116.45365	23.8	335	180	4.0	Strike Slip
	1992.492	0	15	90	34.217	-116.43333	21.8	354	180	3.0	Strike Slip
Hector[c]	1999.792	0	10	90	34.732	-116.382	7.9	165	180	1	Strike Slip
	1999.792	0	10	90	34.664	-116.364	13.9	142	180	3	Strike Slip
	1999.792	0	15	90	34.734	-116.318	26	167	180	3	Strike Slip
	1999.792	0	10	85	34.509	-116.258	9.4	158	180	2	Strike Slip
	1999.792	0	5	80	34.444	-116.230	17	137	180	1	Strike Slip
LittleSkullMtn[c]	1992.496	6.6	12.3	58	36.746	-116.284	6.7	218	-77	0.2	Normal
Kern County[e]											
1	1952.555	5	27	75	35.046	-118.892	27	73	40	3.1	Thrust
2	1952.555	3.5	15	35	35.086	-118.545	27	58	63	2.6	Thrust
3	1952.555	2	10	20	35.170	-118.265	27	43	68	1.1	Thrust
Cedar Mountain[f]											
1	1932.975	0	15	80	38.562	-117.838	15	350	180	1.3	Strike Slip
2	1932.975	0	15	80	38.930	-117.963	60	344	180	2.0	Strike Slip
Ft. Tejon[g]											
1	1857.025	0	20	90	35.734	-120.282	119	135	180	5.0	Strike Slip
2	1857.025	0	20	90	34.930	-119.421	200	112	180	5.0	Strike Slip

Latitude and Longitude Follow VISCO 1D convention, i.e. are coordiantes of bottom corner of fault along strike direction
a) Beanland and Clark, 1994; Pancha et al., 2006
b) Fialko, 2004
c) Fialko et al., 2001
d) Smith et al 2000; Lohman et al., 2002
e) Stein and Thatcher, 1981
f) Bell et al., 1999; Doser, 1988
g) Sieh, 1978